World Scientific
www.worldscientific.com

NIR-II fluorescence imaging in liver tumor surgery: A narrative review

Zihao Liu ®*, Lifeng Yan ®‡, Qingsong Hu ®§ and Dalong Yin ®*,†,¶

*Department of General Surgery, Anhui Provincial Hospital
Anhui Medical University, Hefei 230001, P. R. China

†Department of Hepatobiliary Surgery and Centre for Leading
Medicine and Advanced Technologies of IHM
The First Affiliated Hospital of USTC
Division of Life Sciences and Medicine
University of Science and Technology of China
Hefei, Anhui 230001, P. R. China

‡Hefei National Laboratory for Physical Sciences at the Microscale
CAS Key Laboratory of Soft Matter Chemistry
and Department of Chemical Physics
University of Science and Technology of China, Hefei 230026, P. R. China

§Anhui Province Key Laboratory of Hepatopancreatobiliary Surgery
The First Affiliated Hospital of USTC, Division of Life Sciences and Medicine
University of Science and Technology of China, Hefei 230001, P. R. China
¶doctoryin@ustc.edu.cn

In liver tumor surgery, the recognition of tumor margin and radical resection of microcancer focis have always been the crucial points to reduce postoperative recurrence of tumor. However, naked-eye inspection and palpation have limited effectiveness in identifying tumor boundaries, and traditional imaging techniques cannot consistently locate tumors in real time. As an intraoperative real-time navigation imaging method, NIR fluorescence imaging has been extensively studied for its simplicity, reliable safety, and superior sensitivity, and is expected to improve the accuracy of liver tumor surgery. In recent years, the research focus of NIR fluorescence has gradually shifted from the first near-infrared window (NIR-I, 700–900 nm) to the second near-infrared window (NIR-II, 1000–1700 nm). Fluorescence imaging in NIR-II reduces the scattering effect of deep tissue, providing a preferable detection depth and spatial resolution while significantly eliminating liver autofluorescence background to clarify tumor margin.

¶Corresponding author.

Developing fluorophores combined with tumor antibodies will further improve the precision of fluorescence-guided surgical navigation. With the development of a bunch of fluorophores with phototherapy ability, NIR-II can integrate tumor detection and treatment to explore a new therapeutic strategy for liver cancer. Here, we review the recent progress of NIR-II fluorescence technology in liver tumor surgery and discuss its challenges and potential development direction.

Keywords: Fluorescence guided-surgery; liver cancer; near infrared-II; optical imaging.

1. Introduction

Liver cancer is the seventh most common cancer in the world and the third leading cause of cancer-related death.[1] Hepatocellular carcinoma (HCC), the most common type of liver cancer, has the second low survival rate among all cancers in China.[2] For resectable early and middle-stage liver cancer, hepatectomy is still the most effective treatment for prolonging survival.[3] However, identifying and removing all cancerous tissues is challenging, especially under the consideration of maximizing the preservation of normal liver parenchyma to guarantee adequate remnant liver function. Therefore, there is an urgent need to develop an ideal technique to assist surgeons in achieving the optimal balance between R0 resection and maximum preservation of normal liver tissue.

Near-infrared fluorescence (NIRF) is an emerging imaging technique for real-time intraoperative navigation. Since it was first applied to hepatectomy by Ishizawa *et al.*[4] in 2009, the use frequency of this imaging technique increased rapidly while its role was constantly expanded and modified. Compared with traditional imaging techniques such as computed tomography (CT) or magnetic resonance imaging (MRI), NIRF imaging has the advantages of low cost, easy to use, nonradioactive, high safety, and so forth.[5] According to the spectral wavelength, the near-infrared window includes near-infrared-I (NIR-I, 700–900 nm) and near-infrared-II (NIR-II, 1000–1700 nm). As the main window used for fluorescence imaging at present, NIR-I fluorescence has brought incomparable practicality, efficiency, and precision into surgical scenarios such as lymph node dissection, nerve imaging, and tumor detection.[6,7] Especially in hepatobiliary surgery, *in vivo* fluorescence imaging via NIR-I window provides surgeons with a powerful instrument for real-time navigation, which has manifested its value in detecting primary or metastatic liver tumors, delineating atrophic liver segments and liver transplantation surgery.[5,8,9]

However, confined detection depth and high tissue autofluorescence background limit its practicability in clinical applications.[10] In recent years, studies have proved that the image quality and clinical applicability of NIR-II imaging have significantly improved compared to NIR-I imaging and have preliminarily applied NIR-II to imaging sentinel lymph nodes (SLN) and ovarian tumors.[11,12] Herein, we reviewed and summarized the latest preclinical and clinical progress of NIR-II fluorescence in liver tumor surgery in recent years, and clarified its advantages compared with NIR-I imaging. Finally, the clinical challenges and perspectives for the application of NIR-II fluorescence in liver tumor surgery were discussed.

2. NIR-I to NIR-II: An All-Round Optimization of Fluorescence Imaging

As the first operational window of opening the gate of NIRF imaging, NIR-I has been widely used in various real-time fluorescence navigation surgeries in the past 15 years.[13–17] As a clinical drug approved by the Food and Drug Administration (FDA), indocyanine green (ICG) has excellent water solubility, pharmacokinetics, biosafety, and excellent quantum yield (QY), making it one of the most representative fluorescent dyes in NIR-I imaging. It can be excited by the light of 750–810 nm and emit the light of 830 nm received by the silicon lens.[13] In addition, IRDye800CW, IR-12N3, and other fluorescent groups are also commonly used dyes for NIR-I imaging. The fluorescence imaging mediated by these fluorophores has been used in liver segment staining, tumor imaging, and cholangiography in hepatobiliary surgery, achieving excellent translation in clinical applications.[5,14,15]

Studies have shown that in liver cancer surgery, the fluorescence images produced by NIR-I imaging can exceed the experience of surgeons, indicating suspicious cancerous tissues that cannot be detected by naked-eye inspection and palpation.[4,16] Kudo *et al.*[17] reported that in 32 cases of ICG fluorescence-guided laparoscopic hepatectomy, 17 new lesions that could not be identified with the naked eye were discovered by fluorescence, improving the specificity and sensitivity of tumor detection. He *et al.*[18] conducted a randomized controlled trial to probe into the efficacy of the tumor detection of colorectal liver metastases in NIR-I fluorescence-guided hepatectomies, 64

patients were equally divided into two groups according to whether the operation was guided by ICG fluorescence. The significant differences between ICG group and non-ICG group in the number of tumors detected (3.03 versus 2.28) and 1 year-recurrence (6 versus 15) convincingly proved that NIRF is a more effective imaging method to improve the detection rate of tumors compared with naked eye and traditional preoperative examination. However, the detection depth of NIR-I is only limited to a shallow range and tumors deeper than 8 mm from the liver surface are undetectable.[5] Besides, due to the partial overlap between the NIR-I imaging window and the excitation/emission
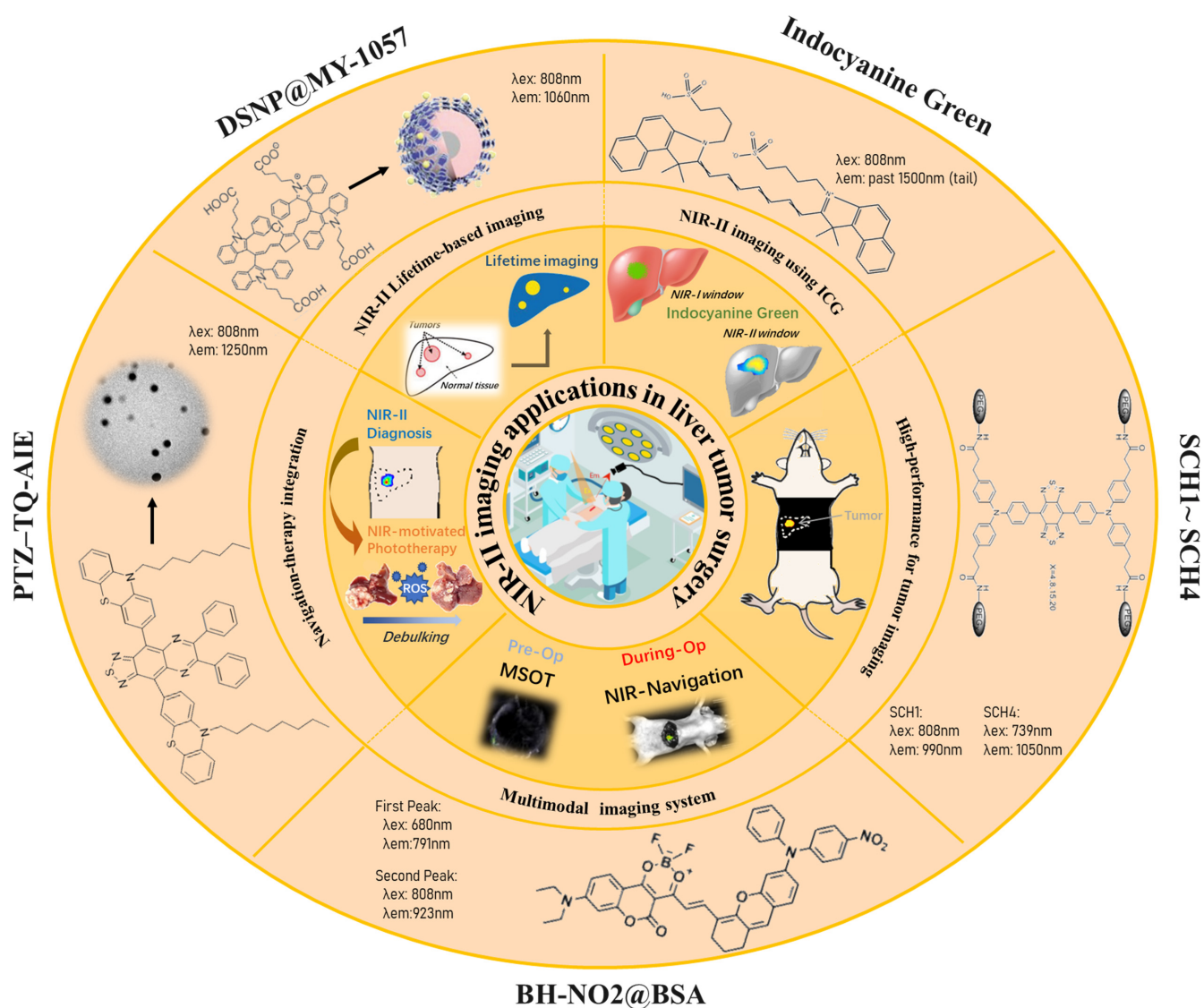
Scheme. 1. Illustrative representation of NIR-II fluorescence imaging technology and its applications in liver tumor surgery. Adapted with permission from Refs. 29, 32, 37, 42 and 45.

Table 1. Studies of NIR-II fluorescence for liver tumor imaging

Reference, Publishing time	Operational window	Experimental subject	Fluorophore	QY, λex/λem	Imaging modality	Target traceability	Tumor location	Image performance, Time post injection	Cell lines
Ding et al.[32] 2018	NIR-II	C57BL/6 mice	SCH1~SCH4	0.14%, 808/990 nm (SCH1) 0.028%, 739/1050 nm (SCH4)	Intensity-based NIRF	Nonspecific	Subcutaneous	SBR 1.8 ~ 1.9, 8 h (SCH1) SBR 7.0 ~ 7.5, 1 h (SCH4)	HepG2
Hu et al.[29] 2020	NIR-I / NIR-II	Human/mice	ICG	N/A, 808 nm/ N/A	Intensity-based NIRF	Nonspecific	Orthotopic	SBR 2.83 ± 1.13,N/A (In human) TNR 2.25 ± 0.06,N/A (In mice)	HepG2
Zeng et al.[37] 2020	NIR-I / NIR-II	BALB/c mice	BH-NO2@BSA	N/A,680/791 nm (FP) 808/923 nm (SP)	Dual-modality NIRF/MSOT	Nitroreductase reaction	Orthotopic	FI (3.0 ~ 3.2)x10^4 a.u., 70 min	HCC-LM3
Ren et al.[39] 2020	NIR-II	NSG mice	Gd-REs@Lips	0.36%,808/1057 nm(FP) 0.17%,808/1335	Dual-modality NIRF/MRI	Nonspecific	Orthotopic	TNR_{NC} 2.1 ± 0.83,N/A	HCC-PDX
Zhao et al.[42] 2020	NIR-II	Mice	DSNP@MY-1057-GPC-3	0.38%o,808/1060 nm	Lifetime-based NIRF	$ONOO^-$ responsive; GPC-3	Orthotopic	LTV of tumor 212 ± 7 ~ 275 ± 49 μs, N/A LTV of normal tissue	HepG2
Jia et al.[45] 2021	NIR-II	BALB/c mice	PTZ-TQ-AIE	0.30%,808/1250 nm	Intensity-based NIRF	Nonspecific	Orthotopic	SNR_{NC},< 5.7'—7.5, 2 h SNR_{PC} 15.5 ~ 16.7,48 h	HepG2
Liao et al.[50] 2021	NIR-II	Nude mice	DCNP coated with IR786s	N/A,980/1550 nm (Stable) N/A,808/1550 nm (ROS induced)	Ratiometric NIRF	NK cell-labeled	Orthotopic	N/A	MHCC97H
Li et al.[48] 2022	NIR-II	Nude mice	CR-PEG-GBP	0.626%, 808/(1000 ~ 1400) nm	Dual-modality NIRF/PAI	GPC-3	Subcutaneous	N/A	HepG2
Shi et al.[30] 2022	NIR-II	Nude mice	GPC3-ICG	N/A,808 nm/ N/A	Intensity-based NIRF	GPC-3	Subcutaneous	TBR 3, 96 h	Huh-7
Lou et al.[34] 2022	NIR-II	Mice	IT-TQT	0.58%, 794/1015 nm	Intensity-based NIRF	Nonspecific	Orthotopic	TNR 1.54, 96 h	143B
Zhang et al.[31] 2022	NIR-II	Human	IgG-IRDye800CW	N/A, 792 nm/ N/A	Intensity-based NIRF	Nonspecific	Orthotopic	Imaging contrast 10.43, 6 days	N/A

Notes: QY, quantum yield; NIRF, near-infrared fluorescence; MSOT, multispectral optoacoustic tomography; MRI, magnetic resonance imaging; SBR, signal-to-background ratio; TNR, tumor-to-normal ratio;N/A, not available; FP, first peak; SP, second peak; FI, fluorescence intensity; PDX, patient-derived xenografts; NC, negative contrast; PC, positive contrast; LTV, lifetime value; SNR, signal-to-noise ratio; DCNP, down-conversion nanoparticles; PAI, photoacoustic imaging.

spectra of some endogenous fluorophores in normal liver tissue,[19] the image of the HCC nodule is vulnerably interfered by liver autofluorescence background, causing a blurry edge of the lesion which is intractable for surgeons to assess. These shortcomings of NIR-I restrict the detecting depth and the clear visualization of tumor boundaries, therefore it is urgent to further expand the imaging window to break through the bottleneck of NIRF.

According to relevant research in recent years, as the near-infrared wavelength extends to the second window (1000–1700 nm), the imaging parameters were significantly improved attributed to the reduced photon absorption and scattering effects at longer wavelengths, offering a centimeter-level penetration depth to the maximum, the maximum depth at which micrometer-level spatial resolution can be obtained has been increased to 3 mm, which is significantly higher than that of NIR-I, making it possible to resolve the underlying anatomical features in a deeper level.[20] Moreover, the higher wavelength threshold of NIR-II could filter and block the autofluorescence background from normal liver parenchyma to achieve the optimal contrast delineation of tumors.[10,21,22] The emergence of NIR-II is a critical upgrade to the powerful real-time fluorescence navigation technique, which is expected to boost the eradication and effectiveness of liver tumor surgery and prolong patients' disease-free survival. In this paper, the reported NIR-II fluorescent agents designed for HCC imaging and their properties are summarized in Table 1. Applications of NIR-II fluorescence imaging for liver tumor surgery are illustrated in Scheme 1.

3. Applications of NIR-II Fluorescence in Liver Tumor Surgery

3.1. *NIR-II imaging mediated by NIR-I fluorophores*

The clinical translation of NIR-II navigation surgery has been hampered by a shortage of fluorophores that are allowed to be used in the human body. Although some dyes such as carbon nanotubes and small molecule dyes have been developed and showed great potential in NIR-II, they are still in clinical trials.[23,24] Fortunately, it has been proposed that some NIR-I agents with a longer emission wavelength such as ICG, IRDye800CW, and IR-12N3 show emission tails reaching past 1000 nm

in NIR-II window (Fig. 1(A)).[25–27] Starosolski *et al.* confirmed that ICG, which was the most representative dye in NIR-I bioimaging, also can be used for high-quality imaging in the NIR-II window.[28] These conclusions indicate that the implementation of NIR-II bioimaging may not necessitate the exclusive use of dyes whose peak emission is located in the NIR-II spectrum. Traditional NIR-I agents with a long emission tail extending to NIR-II window also provide a shortcut, which can greatly accelerate the clinical application of NIR-II imaging. In 2019, a multispectral imager integrated with visible light, NIR-I, and NIR-II was built for the first-in-human study of a group of 23 patients with liver cancer (Fig. 1(B)).[29] Intraoperative fluorescence imaging was performed using ICG to acquire the NIR-I/II images and the white light images of the operation area simultaneously through this integrated system (Fig. 1(C)). The key indicators of tumor images such as signal-to-background ratio (SBR), tumor-to-background ratio (TBR), and tumor-to-normal tissue ratio (TNR) are quantitatively analyzed and compared in two different near-infrared imaging windows. The comparative analysis unequivocally demonstrated a comprehensive superiority of NIR-II over NIR-I in the imaging efficacy of tumors. What counts more is NIR-II imaging newly indicated three tumors that were omitted by NIR-I (Fig. 1(D)). Moreover, the sensitivity and specificity of tumor detection via NIR-II window are nearly 10 percentage points higher than those achieved with NIR-I imaging. Being able to detect the lesions missed by NIR-I, NIR-II undoubtedly promotes the accuracy and radical effect of tumor surgery to a higher level. This progress is likely to change the patient's staging, prognosis, and treatment to reduce the probability of postoperative recurrence and prolong the survival time. Real-time fluorescence navigation surgery via the NIR-II window enables the surgeon to obtain tumor images with higher resolution and target-to-background contrast to delineate the tumor margin more precisely. In addition, according to the above study, NIR-II imaging has better discrimination among primary liver carcinoma nodules, intrahepatic and extrahepatic metastases and is more sensitive in distinguishing different pathological types and differentiated degrees of liver cancer nodules, which may become another valuable information for surgeons to initially evaluate liver tumors intraoperatively shortly (Fig. 1(E)). The superiority of NIR-II
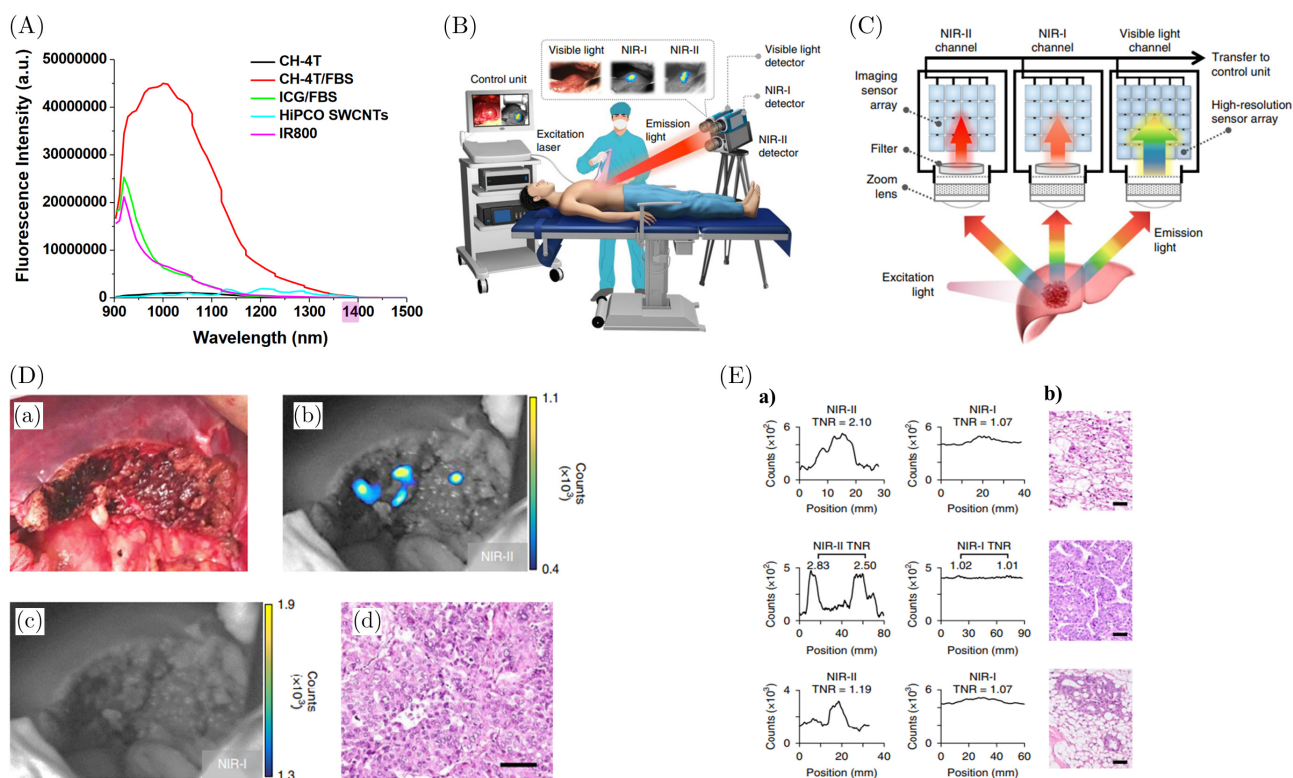
Fig. 1. (A) Fluorescent emission of NIR-I/II dyes past 1000 nm. Emission spectrum at wavelengths longer than 900 nm after 808 nm laser excitation from NIR-II fluorophores including CH-4T, CH-4T/FBS and HiPCO carbon nanotubes as well as NIR-I dyes such as IR800 and ICG/FBS. Adapted with permission from Ref. 25. (B) The liver surface was examined by the integrated NIR-I/II and visible multispectral imaging instrument and visible and NIR-I/II images were obtained. Adapted with permission from Ref. 29. (C) Schematic of the integrated visible and NIR-I/II multispectral imaging instrument. Adapted with permission from Ref. 29. (D) (a) For a typical patient with HCC, guided by ultrasonography and the visible light image, the tumor was resected and thought to be completely removed on the basis of the experience of the surgeons. (b) NIR-II imaging detected fluorescence signals in the remaining tissue sections. (c) NIR-I imaging did not reveal any signals. (d) The fluorescent residual tissues were further resected and received histopathological examination to verify that the tissues were HCC. Adapted with permission from Ref. 29. (E) (a) The quantitative analysis results also showed that the NIR-II imaging discriminated a nodule of liver cancer more effectively compared with NIR-I. (b) The H&E results showed that the tumors were well-differentiated HCC (top), moderately differentiated HCC (middle) and ICC (bottom). Reproduced with permission from the publisher. Adapted with permission from Ref. 29.

imaging is also reflected in the capacity of resisting disturbance from the lighting condition of the operating room, while NIR-I imaging can only operate normally when the lighting is turned off. Otherwise, the imaging clarity will greatly reduce, indicating that NIR-II imaging is more suitable for the lighting conditions of the operating room. However, utilizing the emission tail of ICG for NIR-II imaging remains constrained by certain limitations. As a nontargeted fluorophore, the accumulation of ICG in benign lesions can interfere with the sensitivity and specificity of malignant liver tumor detection, leading to false-positive results. Shi *et al.* conjugated ICG with GPC-3 antibodies to develop fluorescence probe, GPC-ICG, targeting HCC.[30] In a subcutaneous Huh-7 tumor mouse model expressing GPC-3,

NIR-II imaging revealed that the GPC3-ICG probe specifically accumulated in tumors, distinctly delineating the tumor from surrounding tissue. In contrast, the control group, using IgG-ICG, exhibited a weaker fluorescence signal, demonstrating the liver cancer targeting capability of the probe. Furthermore, Zhang *et al.* synthesized the nanoprobe IgG-IRDye800CW and employed a negative staining tumor imaging strategy during hepatectomy in a 66-year-old male patient with HCC and liver cirrhosis.[31] This approach aimed to address the false positives often encountered in liver cancer detection using conventional dyes like pure ICG and IRDye800CW. The negative staining imaging strategy resulted in the tumor area being nonfluorescent, while normal liver parenchyma and

cirrhotic lesions fluoresced, successfully guiding the resection of liver cancer with liver cirrhosis. These strategies facilitate the clinical application of NIR-I fluorophores. However, to fully exploit the potential of NIR-II imaging, the development of dyes with emission peaks over 1000 nm presents a more promising avenue. The advancements in imaging quality using NIR-I fluorophores in NIR-II window can be attributed to improved tissue penetration and reduced biological tissue scattering, which overshadow the diminished fluorescence brightness of NIR-I fluorophores.

3.2. *High-performance of tumor imaging*

CH1055, a novel small-molecule dye developed by Antaris *et al.* in 2016, shows excellent imaging quality *in vivo*.[23] Since its appearance, it has become one of the most representative NIR-II dyes with excitation and emission wavelengths located at 750 and 1055 nm, respectively. Due to its excellent performance both in biocompatibility and function-plasticity, CH1055 is widely used as a small-molecule dye platform for renovation. Ding *et al.* constructed a class of NIR-II agents based on CH1055 conjugating with a series of short

polyethylene glycol (PEG) linkers, named SCH1–SCH4.[32] Through the creative PEGylation strategy, this class of dyes is not only endowed with good solubility and low biotoxicity for bioimaging but also the assembled size can be regulated by adjusting conjugated functional groups, ranging from nanoparticle (NP) to molecule (Fig. 2(A)). Previous studies have demonstrated that fluorescence agents conjugating with PEG linkers would remarkably improve the pharmacokinetics and tumor uptake thanks to the acceleration of the nonspecific diffusion and accumulation in the tumor microenviroment.[11,23,33] The consequence of subsequent NIR-II fluorescence imaging of xenograft HepG2 tumors in mice further proved this point. Ten min after intravenous injection of SCH4, which possesses the best balance between photostability and urine excretion rate *in vivo* among the four agents, the tumor was noticeably different from the surrounding normal tissue (Fig. 2(B)). Until 1 h, the TNR of the tumor image reached the maximum, with an astonishing value of 7.2 (Fig. 2(C)). The ability to provide images of high TNR value will undoubtedly improve the recognition of the tumor margin and the positive rate of microcancerous lesions, making fluorescence-guided tumor surgery more precise and radical. Lou *et al.* developed a
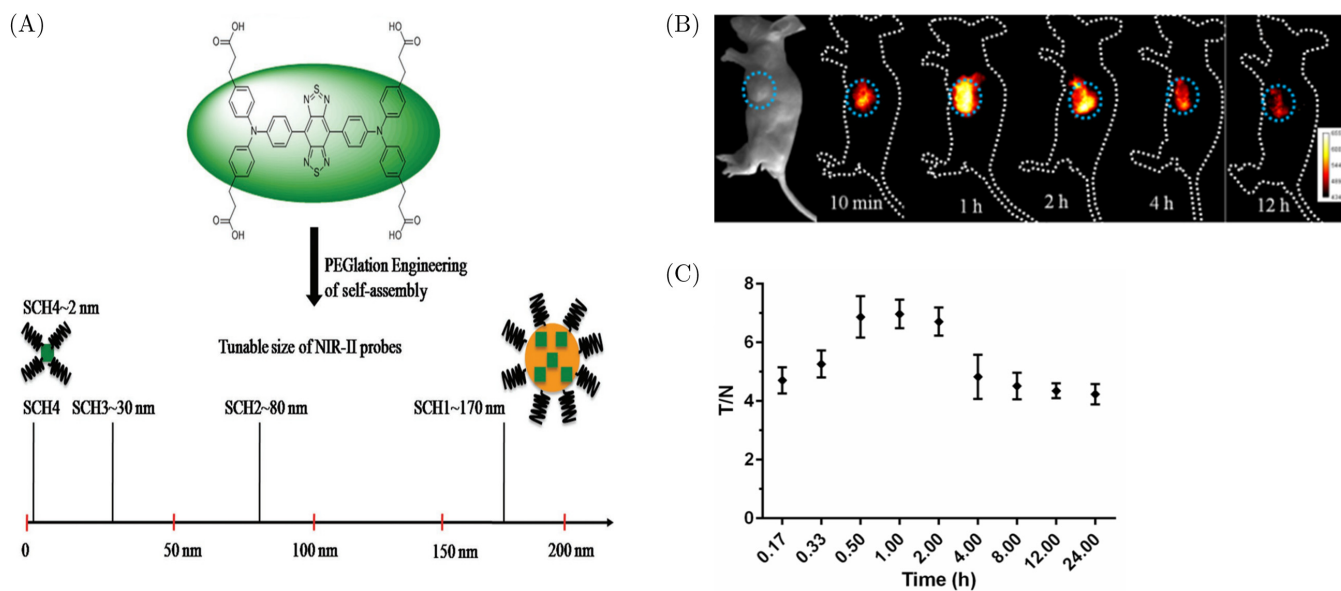

Fig. 2. (A) Facile PEGylation strategy for regulating the assembly of NIR-II probes based on a CH1055 platform (SCH1–SCH4), with sizes ranging from single molecule to nanoparticle. Adapted with permission from Ref. 32. (B) HepG2 tumor-earing mice imaging in the NIR-II window at 10 min, 1 h, 2 h, 4 h, 12 h after intravenous injection of SCH4. Adapted with permission from Ref. 32. (C) T/N ratios acquired at different time points. Reproduced with permission from the publisher. Adapted with permission from Ref. 32.

small molecule NIR-II dye, IT-TQT, encapsulated it within DSPE-PEG2000, forming IT-TQT NPs for NIR-II imaging.[34] These IT-TQT NPs demonstrated remarkable capabilities in the detection of ultra-small liver metastasis, as small as 90 μm, in a mouse model. Differing from the SCH4, the IT-TQT molecules encapsulated in liposomes resulted in an increased size, predominantly clearing via hepatobiliary pathway, with minor renal system clearance. This high liver uptake resulted in a lower TNR of liver metastasis, with a maximum TNR of 1.54. Given the physiological functions of metabolism, detoxification and phagocytosis of liver, these nanoscale fluorescence probes are often nonspecifically uptaken by the reticuloendothelial system (RES) of liver post intravenous administration. This uptake can interfere with the fluorescence signal in the tumor site, making it difficult to achieve imaging results and quality in orthotopic liver tumor models comparable to subcutaneous tumor models. Therefore, controlling factors like molecular weight and particle size that influence the pharmacokinetic properties of the fluorophores is imperative to realize high-quality NIR-II imaging in orthotopic liver tumors.

3.3. *Multimodal systems based on NIR-II*

Attaining high resolution and contrast concurrently has always been one of the paramount objectives in bioimaging research. In recent years, the multimodal imaging system combining NIRF with traditional imaging techniques has gradually attracted close attention.[35,36] Multi-modal imaging, integrating two or more imaging modalities, capitalizes on the complementary capabilities of different imaging methods to provide comprehensive information on tumor regions across diverse spatial scales. While significant advancements in NIR-II fluorescence imaging have been made in recent years, it inherently lags in terms of penetration depth and axial resolution when compared to MRI, CT, positron emission tomography (PET), single-photon emission computed tomography (SPECT), and photoacoustic imaging (PAI). Among these techniques, MRI and CT generate high-resolution anatomical images, albeit with low contrast agent sensitivity. PET and SPECT boast nearly unrestricted penetration depths, high sensitivity, and quantitative capabilities, but with limited spatial resolution.

PAI offers strong contrast and high 3D spatial resolution at centimeter-level penetration depths. However, its acquisition of volumetric data is intricate and time-consuming, with a reduced temporal resolution hampering real-time surgical guidance.[22] Thus, there is a pressing need to develop NIR-II-based multimodal imaging strategies to counterbalance the inherent limitations of standalone NIR-II imaging. Traditional imaging methods also need the micron-scale spatial resolution, high time resolution, excellent operability, and capabilities of low-latency real-time guidance provided by the NIR-II imaging to maximize the functional extension.

Zeng *et al.* designed an activatable nanoprobe, BH-NO2@BSA, with dual-modal imaging functions of NIR-II fluorescence and multispectral optoacoustic tomography (MSOT).[37] The nanocomposite probe can specifically react to the highly-expressed nitroreductase of liver tumor cells and give out significant fluorescence at the NIR-II window after being activated (Fig. 3(A)). Different from the traditional inert probe, the activable probe emits a fluorescence signal only when it encounters or reacts with the target biomarkers, effectively reducing the background fluorescence and improving the sensitivity of liver tumor detection.[38] Moreover, the activated probe becomes an ideal photo absorber for MSOT imaging through which can obtain the 3D image of the tumor to enrich the preoperative imaging preparation (Fig. 3(B)). With a large amount of valuable information provided by MSOT and a real-time fluorescence navigation system, the accuracy of liver tumor surgery can be further improved. Similarly, Ren *et al.* reported a rare earth-doped NP Gd-REs@Lips which has performed a good T2 weighted contrast effect via MRI (Fig. 3(C)).[39] Meanwhile, it is also regarded as a promising agent for NIR-II imaging owing to its innate structural features such as large Stokes shift, multi-peak emission, and prominent light stability.[40] Interestingly, the study reported an unusual isolation strategy of liver tumors based on the interaction of RES other than bile excretion disorder and molecular marker targeting. Images obtained *in vivo* showed that NIR-II signal from Gd-REs@Lips was mainly concentrated in normal liver tissue, while the tumor region presented no signal, resulting in a negative image of the tumor with a clear distinction from the surrounding tissue (Fig. 3(D)). Phagocytosis of macrophages abundant in the liver might be the possible mechanism for this phenomenon.[35]
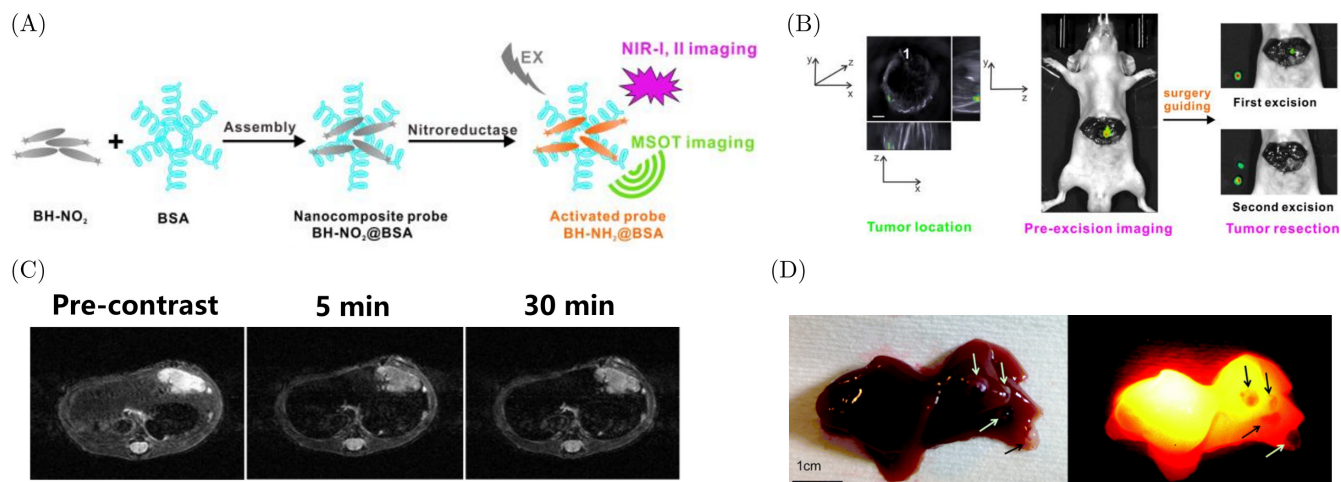
Fig. 3. (A) Schematic illustration of the formation of the nanocomposite probe BH-NO2@BSA and its response to nitroreductase. Adapted with permission from Ref. 37. (B) Location of orthotopic liver tumor achieved by 3D MSOT imaging and the imaging-guided tumor resection surgery by NIR fluorescence imaging using the nanocomposite probe. Reproduced with permission from the publisher. Adapted with permission from Ref. 37. (C) T2-weighted images of mice before, 5 min and 30 min after tail vein injection of Gd-REs@Lips. Adapted with permission from Ref. 39. (D) Satellite liver lesions on the liver surface (arrows) (Left: White light image; Right: NIR-II image). Adapted with permission from Ref. 39.

In such high-contrast images, some satellite lesions with a minimum diameter of 2 mm that could have been easily neglected by visual diagnosis can be effectively detected. Sun *et al.* reported an integrated NIR-II/PET multimodal small-molecule based $\alpha_V\beta_3$-targeted probe ^{68}Ga-CHS2, indicating the maximum emission wavelength at 1055 nm.[41] The ^{68}Ga^{3+} in the probe serves as a radioactive label, achieving tumor PET imaging. Upon intravenous injection, the small molecule probe demonstrated pronounced tumor accumulation, resulting in a distinct contrast in NIR-II/PET imaging compared to normal tissues. Subcutaneous glioma-derived tumors were preoperatively detected via PET imaging and subsequently completely excised under the precise delineation of real-time NIR-II imaging. Additionally, the pharmacokinetics of ^{68}Ga-CHS2 demonstrated renal and hepatobiliary excretion, such multimodal small-molecule probes with the ability of rapid metabolism *in vivo* hold immense potential for preoperative diagnostic evaluation and precise image-guided surgery in the future for hepatic tumors.

3.4. *Novel lifetime-based NIR-II imaging*

There is no doubt that NIR-II imaging has pushed the detection rate of liver tumors to another level, especially in the superficial layer of the liver.

However, due to signal attenuation caused by heterogeneous scattering and absorption within tissues, the imaging accuracy of intensity-based NIR fluorescence imaging diminishes progressively with increasing depth of tumors.[19] Zhao *et al.* proposed a neoteric NIR-II lifetime-based fluorescence imaging method.[42] This approach, slightly divergent from the commonly employed intensity-based imaging principle, ensures consistent lifetime responses within its detectable depth range. Compared to intensity-based imaging, where signal attenuation escalates with increasing depth, this lifetime-based imaging maintains stable lifetime values across various depths, ensuring the reliability of physiological data acquired at different tissue depths.

Zhao *et al.* established a NIR-II lifetime-based ONOO-responsive nanosensor using a lanthanide–cyanine FRET (fluorescence resonance energy transfer) system. Besides, targeting antibody glypican-3 (GPC-3) was attached to the nanosensor to enhance traceability. Through the detection of ONOO−, which is closely related to the tumor microenvironment, cancerous tissue could be distinguished from liver parenchyma (Fig. 4(B)).[43,44] More advantageously, no matter what the penetration depth is, the lifetime NIR-II imaging intensity is always linear with the concentration of ONOO$^-$, which means richer tumor information can be provided by quantifying the index of ONOO$^-$ (Fig. 4(A)). Finally, the ability of
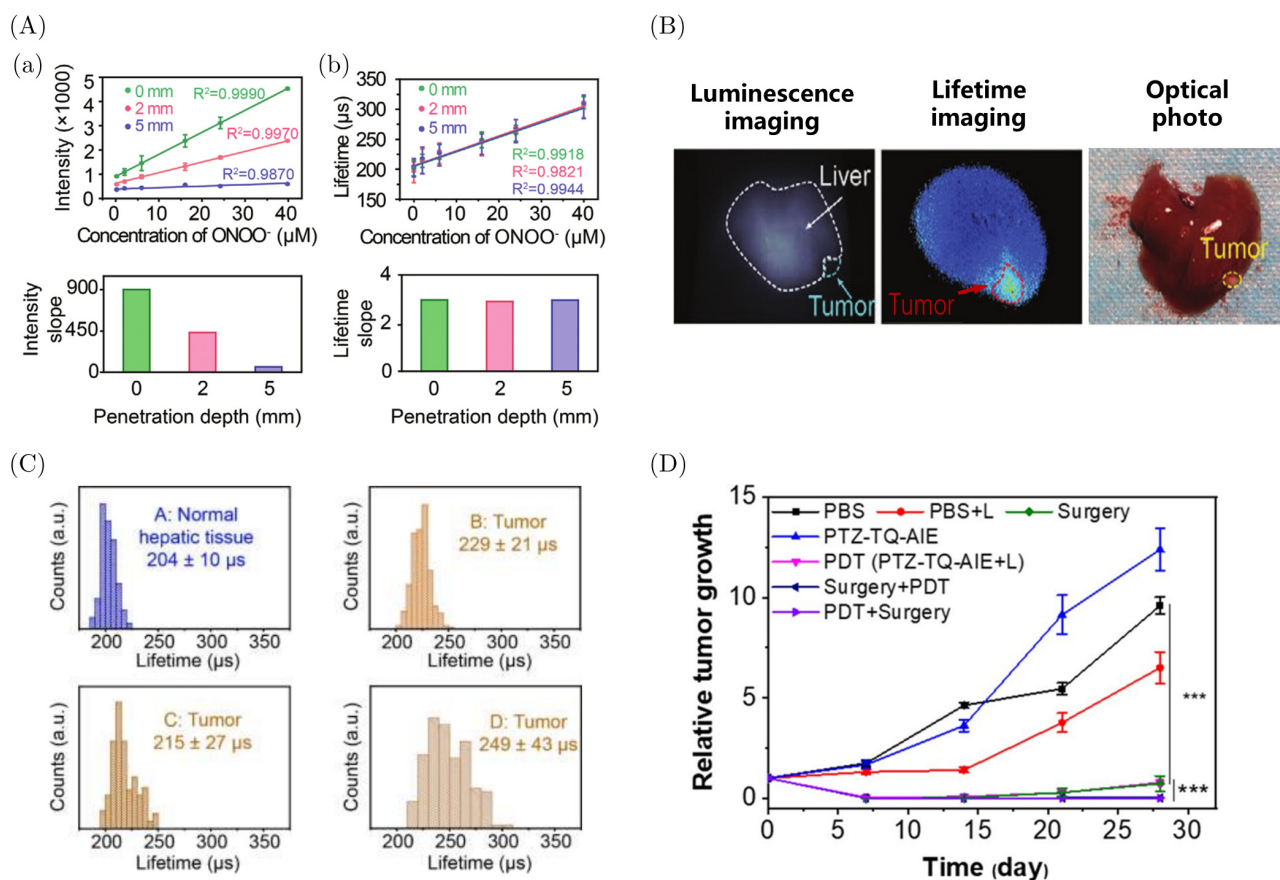
Fig. 4. (A) Intensity- and lifetime-based imaging results as a function of ONOO$^-$ concentration with DSNP@MY-1057-GPC-3 contained capillaries under different penetration depths. (a) The fluorescence intensity-ONOO$^-$ concentration slope varies with depth, (b) the lifetime value-ONOO$^-$ concentration slope is always consistent. Adapted with permission from Ref. 42. (B) Non-invasive intensity-based imaging, lifetime-based imaging of HCC-bearing mice and optical photo of dissected livers. Tumor lesions and normal hepatic tissues are marked as indicated. Adapted with permission from Ref. 42. (C) Lifetime distribution of multiple HCC lesions (marked as (B)–(D)) in mouse, (A): normal hepatic tissue; (B)–(D): tumor lesions. Reproduced with permission from the publisher. Adapted with permission from Ref. 42. (D) The relative tumor growth curve of the tumor-bearing mice under different treatment strategies. Surgery+PDT: Applying surgery first and then PDT treatment for the residual tumors; PDT+Surgery: Applying PDT treatments to reduce the tumor size first then conducting surgery to minimize the injury of the liver in the therapeutic process. Reproduced with permission from the publisher. Adapted with permission from Ref. 45.

tumor-delineating of lifetime imaging was tested by establishing a multiple HCC model. The reliability of the lifetime-based detection method was verified by the distinctiveness between three lesions and normal liver tissue ($215 \pm 27 \sim 249 \pm 43 \mu$s versus $204 \pm 10 \mu$s) as well as the highly coincident signal with MRI imaging and white light image (Fig. 4(C)). However, it is important to note that while fluorescence lifetime imaging provides consistent lifetime responses within its detection depth limit, exceeding this range may result in significantly weakened fluorescence signals due to scattering and absorption, leading to inaccuracies and nonresponsiveness in lifetime value acquisition.

3.5. *Navigation-therapy integration via NIR-II fluorescence*

The advanced optical principle of NIR-II not only brings the progress of tumor visualization intraoperatively but also breaks through the "single-function positioning" limitation of NIR-II in liver cancer surgery. In addition to the function of tumor visualization, NIR-II imaging also has an unfathomable potential in tumor phototherapy. Jia *et al.* designed a NIR-II photosensitizer, PTZ-TQ-AIE, based on aggregation-induced-emission (AIE) feature and tested its near-infrared imaging ability and photodynamic therapy (PDT) efficacy in mice models.[45] What is more advanced than the previous

NIR-II phototherapy strategy is that PTZ-TQ-AIE possesses a dual function of photoluminescence and reactive oxygen species (ROS) generator, which does not require NIR agents-photosensitizers coupling. This feature has been proved to be able to achieve the best therapeutic effect in NIR-II guided phototherapy surgery.[46] More significantly, the models of multiple small HCC and large HCC were constructed to simulate possible cases in the real clinical environment. Usually in practice, the surgical resection feasibility for such tumors is restricted due to their high recurrence rate after the surgery. Given this situation, the researchers formulated different treatment protocols. For multiple small HCC, the NIR-II fluorescence surgical resection was first conducted followed by PDT treatment toward the residual lesions. As for large HCC, PDT was first applied to the size of tumor to ensure sufficient remnant functional liver volume after the surgery. The result showed that the combination of NIR-II photosensitizer-mediated phototherapy and fluorescence-guided surgery significantly reduced tumor recurrence compared with the control group (Fig. 4(D)), creating an opportunity for positive treatment for advanced liver cancer.

The heat generated upon the excitation of fluorescent dyes can also serve as a phototherapeutic means for HCC. NIR-II fluorophores with efficient photothermal conversion capabilities can transform the absorbed light energy into thermal energy, producing elevated temperatures that lead to tumor cell death. Dang *et al.* were the first to introduce hydrogen bonding into BODIPY, constructing J-aggregates through intermolecular hydrogen bonding and π–π stacking interactions, achieving NIR-II fluorescence emission and high photothermal conversion efficiency (PCE = 55%). In subcutaneous liver cancer models, they realized galactose-targeted NIR-II imaging and photothermal therapy (PTT), effectively ablated the tumors.[47] Li *et al.* developed a GPC-3 targeted probe, CR-PEG-GBP, that achieves dual-modal imaging through NIR-II fluorescence and photoacoustic modalities, and guides PTT and sonodynamic therapy (SDT) for HCC.[48] Upon actively targeting subcutaneous HepG2 tumors, CR-PEG-GBP responds to the acidic tumor microenvironment by self-assembling into NPs, thereby enhancing tumor accumulation and retention. Under the guidance of NIR-II fluorescence and PAI, CR-PEG-GBP mediated PTT and SDT exhibit synergistic tumor suppression effects.

Hu *et al.* developed the DOX@PEG-Ag$_2$S nanoplatform, integrating drug delivery, tumor microenvironment-responsive drug release, and NIR-II imaging. Adopting a passive targeting strategy, doxorubicin (DOX) can be rapidly released in the acidic environment within tumors to inhibit growth. Simultaneously, the NIR-II fluorescence generated by Ag$_2$S QD is used for real-time assessment of the therapeutic effect on subcutaneous breast tumors, enriching personalized tumor diagnosis and therapy.[49] NIR-II based therapeutics represent a promising photo-controlled drug delivery approach, offering real-time visual feedback on the *in vivo* targeting process and therapeutic outcomes of chemotherapeutic agents, expected to facilitate the research of targeted immunotherapy for liver cancer. To avoid potentially harmful excessive thermal effects during the visualized process, transient and intermittent NIR-II excitation may be a feasible solution.[22] Liao *et al.* developed a ratiometric NIR-II fluorescence imaging strategy for real-time quantitative tracking and visualization of the viability of adoptive NK cells in an orthotopic HCC model.[50] The nanoreporter consists of lanthanide-based down-conversion nanoparticles (DCNP) coated with IR786s. Upon cell death, the generation of ROS disrupts the absorption competition-induced emission (ACIE) balance between DCNP and IR786s, resulting in an enhanced fluorescence signal from DCNP under 808 nm excitation, while the fluorescence signal under 980 nm excitation remains unchanged. This alteration in the ratio of the two fluorescence signals indirectly reflects the viability of NK cells. Furthermore, leveraging this nanoreporter, the co-treatment with IL-2, IL-15, and IL-21 has been demonstrated for the first time to enhance the *in vivo* viability and implantation efficiency of NK cells, thereby improving the therapeutic efficacy against orthotopic HCC.

4. Challenges and Perspectives

NIR-II fluorescence imaging has shown strong potential to improve clinical outcomes through its superior imaging capability and application expansibility. It is undeniable that by switching the optical window, the progress of NIR-II in detection depth makes the clinical translation of this technique in liver cancer surgery greatly leap forward. However, due to the congenital disadvantage of optical imaging, which is susceptible to photon

refraction and absorption, it still focuses on a relatively superficial depth compared with ultrasound detection when dealing with deeper liver tumors. Therefore, the necessity of intraoperative ultrasound and preoperative traditional imaging examination should also be emphasized to minimize the possibility of missing primary or metastatic lesions. In addition to recourse to the traditional imaging techniques, NIR-II lifetime imaging or the combination with PAI can also be a viable option for the depth constraint, which is also a promising development direction in the future. With the exploration of dual-mode probes in recent years, more tumor anatomy information can be unearthed.[37,40] Preoperative photoacoustic info and intraoperative real-time fluorescence navigation may confirm and complement each other to reach the ultimate utilization of the profound potential of the NIR-II fluorescence imaging, bringing the completeness of liver cancer surgery to another stage.

Compared to NIR-I, NIR-II can significantly reduce the liver fluorescence background while highlighting the tumor to achieve the optimum contrast, but it does not mean that all distractions affecting tumor visualization are ruled out. It also depends on the characteristics of the chosen fluorophores. Using ICG for NIR-II imaging adheres to the nonspecific mechanism of bile excretion disorder, which is susceptible to interference from cirrhotic nodules, causing false-positive conditions. It is easy to lead surgeons to expand the scope of surgical resection. Since the liver compensatory capacity of patients with liver cirrhosis is usually impaired, the risk of liver insufficiency and various complications after the expanded resection will be further increased. As for some novel NP agents using the discrepancy between normal liver and tumor in the RES to achieve negative contrast imaging, their effect remains dubious to be guaranteed due to the heterogeneity of tumor cells. A promising way to isolate these interferences is to enable fluorophores with target-tracking capabilities. Currently, most developed NIR-II agents are nonspecific to liver tumors, limiting the efficiency of accurately delineating cancerous lesions in fluorescence-guided surgery. Conjugation with specific biomarkers could be one of the effective solutions to empower tumor-tracking capability. Clinically employed biomarkers for early-stage diagnosis of HCC, such as alpha-fetoprotein (AFP), AFP-L3, Golgi protein 73 (GP-73), heat shock protein 70

(Hsp70), and des-γ-carboxy prothrombin (DCP), present potential suitable sites for HCC-specific fluorescent targeted imaging. However, when designing a targeting conjugation strategy, critical considerations include the marker's specific cellular localization, differential expression between malignant tumor and normal tissues, and solubility and stability in the circulation. While the levels of AFP, AFP-L3, and DCP are typically elevated in patients with HCC, their high solubility in the blood might contribute to nonspecific background signals, compromising the specificity and sensitivity of the imaging. Given that GP-73 is a membrane protein, it might theoretically offer a more suitable site for fluorophore conjugation compared to Hsp70, which is primarily localized in the cytoplasm and nucleus. Membrane proteins such as GPC-3, CXCR4, and integrin $\alpha6$ have been reported as highly selective biomarkers with potential for HCC diagnosis, holding promise as ideal target proteins for HCC-specific imaging.[51–53] Nevertheless, the performance of these biomarkers in NIR-II liver tumor imaging still requires further experimental validation. Additionally, the specific biochemical reaction between tumor microenvironment and fluorophores paves a new path toward tumor targeting in the absence of liver cancer biomarkers. By binding well-designed chemical groups, the probe can be readily taken up by liver and specifically respond to the particular abnormal pH, redox, or enzyme generated in the tumor microenvironment and then the structure of the fluorophore changes to an activated state to fluoresce.[54–56] Tang *et al.* proposed an innovative double-lock strategy to perform ultrahigh-specific fluorescence imaging of tumors *in vivo*.[57] They developed a dual-pathological-parameter cooperatively activatable nanoprobe making use of the overexpressed hyaluronidase (Hyal) and thiols in tumor to activate the probe, and thus efficiently reduced nonspecific activation and the liver fluorescence background.

In addition to the achievements in visual enhancement, the great potential of NIR-II fluorescence in liver cancer PTT/PDT or chemo/immunotherapy should not be neglected. The integrated platform of NIR-II fluorescence diagnosis-treatment will become a development trend in the future clinic and has received great interest from researchers by virtue of high transmittance, controllable behavior, subtle damage to normal tissues, and, most importantly, the real-time ability to

identify microcancerization.[58,59] NIR-II fluorophores with excellent photothermal conversion efficiency and high ROS generation rate have been developed in recent years[45,60] Integrating NIR-II with PTT can be a strong competitor of radiofrequency ablation to enrich the available options for liver cancer treatment, but the change of prognosis remains to be confirmed by clinical trials. The integration of NIR-II/ PDT can be used not only for preoperative noninvasive neoadjuvant down-stage therapy of huge HCC without surgical indication, but also for intraoperative elimination of multiple small tumor foci. In terms of chemo/immunotherapy, a variety of drug-fluorescent complexes have been developed,[50,61] which can be activated in specific tumor areas, ensuring the least systemic adverse events. According to the research, NIR-II fluorescence intensity has also been found to correlate well with drug concentration, making it possible to visualize drug release at the cellular level and predict the therapeutic effect based on the fluorescence intensity.[61]

5. Conclusions

In vivo imaging experiments in recent years have fully demonstrated the superb performance advantages of NIR-II fluorescence over NIR-I in detection depth, tumor detection rate, and TBR. NIR-II fluorescence-guided liver tumor surgery can not only provide the high resolution of the tumor boundary to help surgeons determine the surgical margins but also prevent the omission of some small disseminated cancer foci that are difficult to be detected by traditional imaging methods and naked eyes, further breaking through the limitation of the curative effect of current liver cancer surgery, fundamentally improving the tumor recurrence rate and long-term prognosis of HCC patients. With the development of a group of fluorophores with excellent photothermal conversion efficiency and high ROS generation rate, NIR-II, with its enhancement in penetration performance, has given a golden timing for clinical translation of NIRF in nonhepatectomy treatment of liver cancer, especially PTT and PDT. Although the optimal biomarkers for HCC binding are still unclear, with many preclinical studies underway, it is foreseeable that the NIR-II targeting probes with excellent pharmacokinetics will be introduced and used in clinical trials for human liver cancer surgery soon.

Conflict of Interest

The authors have no conflicts of interest relevant to this article.

ORCID

Zihao Liu ⓘ https://orcid.org/0000-0002-9398-6942
Lifeng Yan ⓘ https://orcid.org/0000-0002-6063-270X
Qingsong Hu ⓘ https://orcid.org/0000-0002-9765-649X
Dalong Yin ⓘ https://orcid.org/0000-0001-6233-9956

References

1. H. Sung, J. Ferlay, R. L. Siegel, M. Laversanne, I. Soerjomataram, A. Jemal, F. Bray, "Global cancer statistics 2020: GLOBOCAN estimates of incidence and mortality worldwide for 36 cancers in 185 countries," *CA Cancer J. Clin.* **71**(3), 209–249 (2021).
2. C. Xia, X. Dong, H. Li, M. Cao, D. Sun, S. He, F. Yang, X. Yan, S. Zhang, N. Li, W. Chen, "Cancer statistics in China and United States, 2022: Profiles, trends, and determinants," *Chin. Med. J. (Engl).* **135**(5), 584–590 (2022).
3. L. Kulik, J. K. Heimbach, F. Zaiem, J. Almasri, L. J. Prokop, Z. Wang, M. H. Murad, K. Mohammed, "Therapies for patients with hepatocellular carcinoma awaiting liver transplantation: A systematic review and meta-analysis," *Hepatology* **67**(1), 381–400 (2018).
4. T. Ishizawa, N. Fukushima, J. Shibahara, K. Masuda, S. Tamura, T. Aoki, K. Hasegawa, Y. Beck, M. Fukayama, N. Kokudo, "Real-time identification of liver cancers by using indocyanine green

fluorescent imaging," *Cancer* **115**(11), 2491–2504 (2009).

5. A. L. Vahrmeijer, M. Hutteman, J. R. van der Vorst, C. J. van de Velde, J. V. Frangioni, "Image-guided cancer surgery using near-infrared fluorescence," *Nat. Rev. Clin. Oncol.* **10**(9), 507–518 (2013).

6. Q. Y. Chen, J. W. Xie, Q. Zhong, J. B. Wang, J. X. Lin, J. Lu, L. L. Cao, M. Lin, R. H. Tu, Z. N. Huang, J. L. Lin, H. L. Zheng, P. Li, C. H. Zheng, C. M. Huang, "Safety and efficacy of indocyanine green tracer-guided lymph node dissection during laparoscopic radical gastrectomy in patients with gastric cancer: A randomized clinical trial," *JAMA Surg.* **155**(4), 300–311 (2020).

7. R. R. Zhang, A. B. Schroeder, J. J. Grudzinski, E. L. Rosenthal, J. M. Warram, A. N. Pinchuk, K. W. Eliceiri, J. S. Kuo, J. P. Weichert, "Beyond the margins: Real-time detection of cancer using targeted fluorophores," *Nat. Rev. Clin. Oncol.* **14**(6), 347–364 (2017).

8. N. Yokoyama, T. Otani, H. Hashidate, C. Maeda, T. Katada, N. Sudo, S. Manabe, Y. Ikeno, A. Toyoda, N. Katayanagi, "Real-time detection of hepatic micrometastases from pancreatic cancer by intraoperative fluorescence imaging: Preliminary results of a prospective study," *Cancer* **118**(11), 2813–2819 (2012).

9. K. He, X. Hong, C. Chi, C. Cai, K. Wang, P. Li, X. Liu, J. Li, H. Shan, J. Tian, "A new method of near-infrared fluorescence image-guided hepatectomy for patients with hepatolithiasis: A randomized controlled trial," *Surg. Endosc.* **34**(11), 4975–4982 (2020).

10. Kenry, Y. Duan, B. Liu, "Recent advances of optical imaging in the second near-infrared window," *Adv. Mater.* **30**(47), e1802394 (2018).

11. Y. Sun, M. Ding, X. Zeng, Y. Xiao, H. Wu, H. Zhou, B. Ding, C. Qu, W. Hou, A. Er-Bu, Y. Zhang, Z. Cheng, X. Hong, "Novel bright-emission small-molecule NIR-II fluorophores for *in vivo* tumor imaging and image-guided surgery," *Chem. Sci.* **8**(5), 3489–3493 (2017).

12. S. Zhu, S. Herraiz, J. Yue, M. Zhang, H. Wan, Q. Yang, Z. Ma, Y. Wang, J. He, A. L. Antaris, Y. Zhong, S. Diao, Y. Feng, Y. Zhou, K. Yu, G. Hong, Y. Liang, A. J. Hsueh, H. Dai, "3D NIR-II molecular imaging distinguishes targeted organs with high-performance NIR-II bioconjugates," *Adv. Mater.* **30**(13), e1705799 (2018).

13. M. L. Landsman, G. Kwant, G. A. Mook, W. G. Zijlstra, "Light-absorbing properties, stability, and spectral stabilization of indocyanine green," *J. Appl. Physiol.* **40**(4), 575–583 (1976).

14. A. Miyata, T. Ishizawa, K. Tani, A. Shimizu, J. Kaneko, T. Aoki, Y. Sakamoto, Y. Sugawara, K. Hasegawa, N. Kokudo, "Reappraisal of a dye-staining technique for anatomic hepatectomy by the concomitant use of indocyanine green fluorescence imaging," *J. Am. Coll. Surg.* **221**(2), e27–e36 (2015).

15. T. Ishizawa, Y. Bandai, M. Ijichi, J. Kaneko, K. Hasegawa, N. Kokudo, "Fluorescent cholangiography illuminating the biliary tree during laparoscopic cholecystectomy," *Br. J. Surg.* **97**(9), 1369–1377 (2010).

16. Y. M. Zhang, R. Shi, J. C. Hou, Z. R. Liu, Z. L. Cui, Y. Li, D. Wu, Y. Shi, Z. Y. Shen, "Liver tumor boundaries identified intraoperatively using real-time indocyanine green fluorescence imaging," *J. Cancer Res. Clin. Oncol.* **143**(1), 51–58 (2017).

17. H. Kudo, T. Ishizawa, K. Tani, N. Harada, A. Ichida, A. Shimizu, J. Kaneko, T. Aoki, Y. Sakamoto, Y. Sugawara, K. Hasegawa, N. Kokudo, "Visualization of subcapsular hepatic malignancy by indocyanine-green fluorescence imaging during laparoscopic hepatectomy," *Surg. Endosc.* **28**(8), 2504–2508 (2014).

18. K. He, X. Hong, C. Chi, C. Cai, Y. An, P. Li, X. Liu, H. Shan, J. Tian, J. Li, "Efficacy of near-infrared fluorescence-guided hepatectomy for the detection of colorectal liver metastases: A randomized controlled trial," *J. Am. Coll. Surg.* **234**(2), 130–137 (2022).

19. G. Hong, A. Antaris, H. Dai, "Near-infrared fluorophores for biomedical imaging," *Nat. Biomed. Eng.* **1**, 0010 (2017).

20. K. Cheng, H. Chen, C. H. Jenkins, G. Zhang, W. Zhao, Z. Zhang, F. Han, J. Fung, M. Yang, Y. Jiang, L. Xing, Z. Cheng, "Synthesis, characterization, and biomedical applications of a targeted dual-modal near-infrared-II fluorescence and photoacoustic imaging nanoprobe," *ACS Nano.* **11**(12), 12276–12291 (2017).

21. B. Li, L. Lu, M. Zhao, Z. Lei, F. Zhang, "An efficient 1064 nm NIR-II excitation fluorescent molecular dye for deep-tissue high-resolution dynamic bioimaging," *Angew. Chem. Int. Ed. Engl.* **57**(25), 7483–7487 (2018).

22. S. He, J. Song, J. Qu, Z. Cheng, "Crucial breakthrough of second near-infrared biological window fluorophores: Design and synthesis toward multimodal imaging and theranostics," *Chem. Soc. Rev.* **47**(12), 4258–4278 (2018).

23. A. L. Antaris, H. Chen, K. Cheng, Y. Sun, G. Hong, C. Qu, S. Diao, Z. Deng, X. Hu, B. Zhang, X. Zhang, O. K. Yaghi, Z. R. Alamparambil, X. Hong, Z. Cheng, H. Dai, "A small-molecule dye for NIR-II imaging," *Nat. Mater.* **15**(2), 235–242 (2016).

24. J. T. Robinson, G. Hong, Y. Liang, B. Zhang, O. K. Yaghi, H. Dai, "*In vivo* fluorescence imaging in the

second near-infrared window with long circulating carbon nanotubes capable of ultrahigh tumor uptake," *J. Am. Chem. Soc.* **134**(25), 10664–10669 (2012).

25. A. L. Antaris, H. Chen, S. Diao, Z. Ma, Z. Zhang, S. Zhu, J. Wang, A. X. Lozano, Q. Fan, L. Chew, M. Zhu, K. Cheng, X. Hong, H. Dai, Z. Cheng, "A high quantum yield molecule-protein complex fluorophore for near-infrared II imaging," *Nat. Commun.* **8**, 15269 (2017).

26. S. Zhu, B. C. Yung, S. Chandra, G. Niu, A. L. Antaris, X. Chen, "Near-infrared-II (NIR-II) bioimaging *via* off-peak NIR-I fluorescence emission," *Theranostics* **8**(15), 4141–4151 (2018).

27. S. Zhu, Z. Hu, R. Tian, B. C. Yung, Q. Yang, S. Zhao, D. O. Kiesewetter, G. Niu, H. Sun, A. L. Antaris, X. Chen, "Repurposing cyanine NIR-I dyes accelerates clinical translation of near-infrared-II (NIR-II) bioimaging," *Adv. Mater.* **30**, e1802546 (2018).

28. Z. Starosolski, R. Bhavane, K. B. Ghaghada, S. A. Vasudevan, A. Kaay, A. Annapragada, "Indocyanine green fluorescence in second near-infrared (NIR-II) window," *PLoS One* **12**(11), e0187563 (2017).

29. Z. Hu, C. Fang, B. Li, Z. Zhang, C. Cao, M. Cai, S. Su, X. Sun, X. Shi, C. Li, T. Zhou, Y. Zhang, C. Chi, P. He, X. Xia, Y. Chen, S. S. Gambhir, Z. Cheng, J. Tian, "First-in-human liver-tumour surgery guided by multispectral fluorescence imaging in the visible and near-infrared-I/II windows," *Nat. Biomed. Eng.* **4**(3), 259–271 (2020).

30. H. Shi, L. V. Huttad, M. Tan, H. Liu, M. S. Chua, Z. Cheng, S. So, "NIR-II imaging of hepatocellular carcinoma based on a humanized anti-GPC3 antibody," *RSC Med Chem.* **13**(1), 90–97 (2021).

31. Z. Zhang, C. Fang, Y. Zhang, S. Su, B. Li, G. Liu, Z. Hu, J. Tian, "NIR-II nano fluorescence image guided hepatic carcinoma resection on cirrhotic patient," *Photodiagn. Photodyn. Ther.* **40**, 103098 (2022).

32. F. Ding, C. Li, Y. Xu, J. Li, H. Li, G. Yang, Y. Sun, "PEGylation regulates self-assembled small-molecule dye-based probes from single molecule to nanoparticle size for multifunctional NIR-II bioimaging," *Adv. Healthc. Mater.* **7**(23), e1800973 (2018).

33. Q. Li, J. B. White, N. C. Peterson, K. W. Rickert, C. O. Lloyd, K. L. Allen, K. Rosenthal, X. Gao, H. Wu, W. F. Dall'Acqua, M. J. Borrok, P. Tsui, "Tumor uptake of pegylated diabodies: Balancing systemic clearance and vascular transport," *J. Control. Release* **279**, 126–135 (2018).

34. H. Lou, A. Ji, C. Qu, S. Duan, H. Liu, H. Chen, Z. Cheng, "A novel NIR-II nanoprobe for precision imaging of micro-meter sized tumor metastases of

multi-organs and skin flap," *Chem. Eng. J.* **449**, 137848 (2022).

35. T. Ai, W. Shang, H. Yan, C. Zeng, K. Wang, Y. Gao, T. Guan, C. Fang, J. Tian, "Near infrared-emitting persistent luminescent nanoparticles for hepatocellular carcinoma imaging and luminescence-guided surgery," *Biomaterials* **167**, 216–225 (2018).

36. Y. Jin, K. Wang, J. Tian, "Preoperative examination and intraoperative identification of hepatocellular carcinoma using a targeted bimodal imaging probe," *Bioconjug. Chem.* **29**(4), 1475–1484 (2018).

37. Z. Zeng, J. Ouyang, L. Sun, C. Zeng, F. Zeng, S. Wu, "Activatable nanocomposite probe for preoperative location and intraoperative navigation for orthotopic hepatic tumor resection via MSOT and aggregation-induced near-IR-I/II fluorescence imaging," *Anal. Chem.* **92**(13), 9257–9264 (2020).

38. J. Y. Xie, C. Y. Li, Y. F. Li, J. Fei, F. Xu, J. Ou-Yang, J. Liu, "Near-infrared fluorescent probe with high quantum yield and its application in the selective detection of glutathione in living cells and tissues," *Anal. Chem.* **88**(19), 9746–9752 (2016).

39. Y. Ren, S. He, L. Huttad, M. S. Chua, S. K. So, Q. Guo, Z. Cheng, "An NIR-II/MR dual modal nanoprobe for liver cancer imaging," *Nanoscale* **12**(21), 11510–11517 (2020).

40. S. He, S. Chen, D. Li, Y. Wu, X. Zhang, J. Liu, J. Song, L. Liu, J. Q, Z. Cheng, "High affinity to skeleton rare earth doped nanoparticles for near-infrared II imaging," *Nano Lett.* **19**(5), 2985–2992 (2019).

41. Y. Sun, X. Zeng, Y. Xiao, C. Liu, H. Zhu, H. Zhou, Z. Chen, F. Xu, J. Wang, M. Zhu, J. Wu, M. Tian, H. Zhang, Z. Deng, Z. Cheng, X. Hong, "Novel dual-function near-infrared II fluorescence and PET probe for tumor delineation and image-guided surgery," *Chem. Sci.* **9**(8), 2092–2097 (2018).

42. M. Zhao, B. Li, Y. Wu, H. He, X. Zhu, H. Zhang, C. Dou, L. Feng, Y. Fan, F. Zhang, "A tumor-microenvironment-responsive lanthanide-cyanine FRET sensor for NIR-II luminescence-lifetime *in situ* imaging of hepatocellular carcinoma," *Adv. Mater.* **32**(28), e2001172 (2020).

43. X. Ai, Z. Wang, H. Cheong, Y. Wang, R. Zhang, J. Lin, Y. Zheng, M. Gao, B. Xing, "Multispectral optoacoustic imaging of dynamic redox correlation and pathophysiological progression utilizing upconversion nanoprobes," *Nat. Commun.* **10**(1), 1087 (2019).

44. C. Szabó, H. Ischiropoulos, R. Radi, "Peroxynitrite: Biochemistry, pathophysiology and development of therapeutics," *Nat. Rev. Drug Discov.* **6**(8), 662–680 (2007).

45. R. Jia, H. Xu, C. Wang, L. Su, J. Jing, S. Xu, Y. Zhou, W. Sun, J. Song, X. Chen, H. Chen, "NIR-II emissive AIEgen photosensitizers enable ultrasensitive imaging-guided surgery and phototherapy to fully inhibit orthotopic hepatic tumors," *J. Nanobiotechnol.* **19**(1), 419 (2021).

46. Z. Sheng, B. Guo, D. Hu, S. Xu, W. Wu, W. H. Liew, K. Yao, J. Jiang, C. Liu, H. Zheng, B. Liu, "Bright aggregation-induced-emission dots for targeted synergetic NIR-II fluorescence and NIR-I photoacoustic imaging of orthotopic brain tumors," *Adv. Mater.* e1800766 (2018).

47. H. Dang, Y. Tian, Q. Cheng, C. Teng, K. Xie, L. Yan, "Galactose conjugated boron dipyrromethene and hydrogen bonding promoted J-aggregates for efficiently targeted NIR-II fluorescence assistant photothermal therapy," *J. Colloid Interface Sci.* **612**, 287–297 (2022).

48. S. Li, Y. Zhang, X. Liu, Y. Tian, Y. Cheng, L. Tang, H. Lin, "Smart NIR-II croconaine dye-peptide for enhanced photo-sonotheranostics of hepatocellular carcinoma," *Theranostics* **12**(1), 76–86 (2022).

49. H. Feng, L. C. Yan, Z. Y. Jun, W. Mao, W. D. Ming, W. Q. Bin, "Real-time *in vivo* visualization of tumor therapy by a near-infrared-II Ag2S quantum dot-based theranostic nanoplatform," *Nano Res.* **8**, 1637–1647 (2015).

50. N. Liao, L. Su, Y. Zheng, B. Zhao, M. Wu, D. Zhang, H. Yang, X. Liu, J. Song, "*In vivo* tracking of cell viability for adoptive natural killer cell-based immunotherapy by ratiometric NIR-II fluorescence imaging," *Angew. Chem. Int. Ed. Engl.* **60**(38), 20888–20896 (2021).

51. M. Neve Polimeno, C. Ierano, C. D'Alterio, N. Simona Losito, M. Napolitano, L. Portella, G. Scognamiglio, F. Tatangelo, A. Maria Trotta, S. Curley, S. Costantini, R. Liuzzi, F. Izzo, S. Scala, "CXCR4 expression affects overall survival of HCC patients whereas CXCR7 expression does not," *Cell. Mol. Immunol.* **12**(4), 474–482 (2015).

52. F. Zhou, W. Shang, X. Yu, J. Tian, "Glypican-3: A promising biomarker for hepatocellular carcinoma diagnosis and treatment," *Med. Res. Rev.* **38**(2), 741–767 (2018).

53. Y. R. Kim, M. R. Byun, J. W. Choi, "Integrin $\alpha6$ as an invasiveness marker for hepatitis B viral X-driven hepatocellular carcinoma," *Cancer Biomark.* **23**(1), 135–144 (2018).

54. S. Jeong, J. Song, W. Lee, Y. M. Ryu, Y. Jung, S. Y. Kim, K. Kim, S. C. Hong, S. J. Myung, S. Kim, "Cancer-microenvironment-sensitive activatable quantum dot probe in the second near-infrared window," *Nano Lett.* **17**(3), 1378–1386 (2017).

55. G. Xu, Q. Yan, X. Lv, Y. Zhu, K. Xin, B. Shi, R. Wang, J. Chen, W. Gao, P. Shi, C. Fan, C. Zhao, H. Tian, "Imaging of colorectal cancers using activatable nanoprobes with second near-infrared window emission," *Angew. Chem. Int. Ed. Engl.* **57**(14), 3626–3630 (2018).

56. K. Pu, A. J. Shuhendler, J. V. Jokerst, J. Mei, S. S. Gambhir, Z. Bao, J. Rao, "Semiconducting polymer nanoparticles as photoacoustic molecular imaging probes in living mice," *Nat. Nanotechnol.* **9**(3), 233–239 (2014).

57. Y. Tang, Y. Li, X. Hu, H. Zhao, Y. Ji, L. Chen, W. Hu, W. Zhang, X. Li, X. Lu, W. Huang, Q. Fan, ""Dual lock-and-key"-controlled nanoprobes for ultrahigh specific fluorescence imaging in the second near-infrared window," *Adv. Mater.* **30**(31), e1801140 (2018).

58. A. Yuan, W. Huan, X. Liu, Z. Zhang, Y. Zhang, J. Wu, Y. Hu, "NIR light-activated drug release for synergetic chemo-photothermal therapy," *Mol. Pharm.* **14**(1), 242–251 (2017).

59. M. Li, H. Yan, C. Teh, V. Korzh, Y. Zhao, "NIR-triggered drug release from switchable rotaxane-functionalized silica-covered Au nanorods," *Chem. Commun. (Camb.)* **50**(68), 9745–9748 (2014).

60. L. Li, C. Shao, T. Liu, Z. Chao, H. Chen, F. Xiao, H. He, Z. Wei, Y. Zhu, H. Wang, X. Zhang, Y. Wen, B. Yang, F. He, L. Tian, "An NIR-II-emissive photosensitizer for hypoxia-tolerant photodynamic theranostics," *Adv. Mater.* **32**(45), e2003471 (2020).

61. Q. Xie, J. Liu, B. Chen, X. Ge, X. Zhang, S. Gao, Q. Ma, J. Song, "NIR-II fluorescent activatable drug delivery nanoplatform for cancer-targeted combined photodynamic and chemotherapy," *ACS Appl. Bio Mater.* **5**(2), 711–722 (2022).